Journal of Magnetic Resonance **148,** 104–114 (2001)
doi:10.1006/jmre.2000.2214, available online at http://www.idealibrary.com on IDEAL®

Peptide Torsion Angle Measurements: Effects of Nondilute Spin Pairs on Carbon-Observed, Deuterium-Dephased PM5-REDOR

Ingolf Sack,* Yael S. Balazs,* Shai Rahimipour,† and Shimon Vega*,[1]

**Department of Chemical Physics and †Department of Organic Chemistry, Weizmann Institute of Science, Rehovot 76100, Israel*

Received June 12, 2000; revised September 6, 2000

Reintroducing dipolar coupling between spin-1/2 nuclei (e.g., ^{13}C, ^{15}N) and spin-1 ^{2}H, using phase-modulated deuterium dephasing pulses, provides a simple and efficient basis for obtaining peptide backbone torsion angles (ϕ, ψ) in specific stable-isotope enriched samples. Multiple homonuclear spin-1/2 interactions due to isotopic enrichment can arise between neighboring molecules or within a multiply labeled protein after folding. The consequences of ^{13}C homonuclear interactions present during ^{13}C-observed, ^{2}H-dephased REDOR measurements are explored and the theoretical basis of the experimentally observed effects is investigated. Two tripeptides are taken to represent both the general case of $^{2}H^{\alpha}$-alanine (in the tripeptide LAF) and the special case of $^{2}H_{2}^{\alpha}$-glycine (in the tripeptide LGF). The lyophilized tripeptides exhibit narrowed spectral linewidths over time due to reduced conformational dispersion. This is due to a hydration process whereby a small fraction of peptides is reorienting and the bulk peptide fraction undergoes a conformational change. The new molecular packing arrangement lacks homonuclear ^{13}C spin interactions, allowing determination of (ϕ, ψ) backbone torsion angles. © 2001 Academic Press

Key Words: **solid-state NMR; CPMAS; ^{2}H REDOR; rotational resonance; dipolar coupling.**

INTRODUCTION

Solid-state NMR is a unique tool for obtaining molecular level structural details of a wide variety of compounds without inherent restrictions to size or molecular ordering. Specific stable-isotope labeling is an effective strategy for obtaining local structural information in biological systems (reviews: (*1–4*)). An advantage of magic-angle spinning (MAS) solid-state NMR among sophisticated high-resolution structural methods is the flexibility in preparation state of the sample: crystalline, lyophilized, precipitated, membrane-bound, flash-frozen, or frozen solutions are all viable options.

One of the most powerful and widely used MAS methods of modern solid-state NMR is rotational echo double resonance (REDOR) (*5*), which determines heteronuclear distances between spin-1/2 nuclei. The experiments are easy to perform and in most cases the REDOR decay signals can be analyzed with the help of a simple master curve. Internuclear distance measurements between spin-1/2 and spin-1 deuterium (^{2}H) nuclei can be accurately measured using variations of standard spin-1/2 REDOR (*6–12*). The method of PM5-REDOR (*12*) uses optimized phase-modulated pulses to obtain efficient ^{2}H dephasing.

PM5-REDOR was recently used with specific stable-isotope labeling to determine ϕ and ψ peptide torsion angles (*13*). Three peptide torsion angles define the backbone conformation of a protein, (ϕ, ψ, ω). A number of solid-state NMR approaches exist to measure peptide backbone torsion angles and provide definitive information of local protein structure (*14–22*). PM5-REDOR determines peptide backbone conformational angles (ϕ, ψ) by reintroducing ^{13}C–^{2}H or ^{15}N–^{2}H dipolar couplings during MAS using the labeling scheme shown in Fig. 1. Site-specific stable-isotope labeling can be obtained by starting with commercially available enriched amino acids for solid-phase peptide synthesis or for growth medium supplements in bacterial biosynthesis (*23*). The torsion angle, ϕ_i, can be measured by reintroducing the dipolar coupling between a nonexchangeable deuterium at the α-proton position ($^{2}H_i^{\alpha}$) and a ^{13}C-enriched $i-1$ carbonyl carbon. The torsion angle ψ_i is determined in a separate ^{15}N–$^{2}H_i^{\alpha}$ PM5-REDOR experiment between $^{2}H_i^{\alpha}$ and a ^{15}N-enriched $i+1$ amide nitrogen. As in REDOR, every resolved peak in the observed spectrum can be analyzed from one experimental run.

This scheme works well for both two-spin (e.g., $^{2}H^{\alpha}$-alanine) and three-spin ($^{2}H_2^{\alpha}$-glycine) cases. The two-spin ^{15}N–$^{2}H_i^{\alpha}$ PM5-REDOR experiment to obtain ψ_i is sensitive to β-sheet vs α-helical conformations even when signal-to-noise is relatively low. Comparing experimental data and theoretical calculations results in two possible values for L-amino acid torsion angles or four degenerate values of glycine torsion angles. Readily available constraints from Ramachandran plots of ^{13}C–^{15}N REDOR measurements on the same sample can result in unique torsion angles (*13*).

The labeling scheme shown in Fig. 1 is advantageous for extracting multiple structural constraints from a single sample. Four different nuclei can be observed, providing complementary spectroscopic information. The presence of multiple spin

[1] To whom correspondence should be addressed. Fax: +972-8-934-4123. E-mail: civega@wis.weizmann.ac.il.

1090-7807/01 $35.00

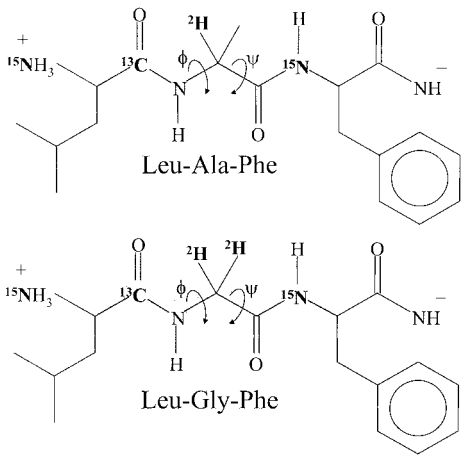

FIG. 1. Site-specific enriched tripeptides were synthesized following standard FMOC chemistry using Rink amide resin and commercially available site-specific deuterated ($^{2}H^{\alpha}$) amino acids (*13*). A $^{13}C_{i-1}$–$^{2}H_{i}^{\alpha}$ PM5-REDOR distance measurement results in the conformational angle ϕ_i, similarly a $^{15}N_{i+1}$–$^{2}H_{i}^{\alpha}$ distance measurement results in ψ_i.

pairs can be problematic and complicates analyses, although new experimental procedures were recently developed toward multiple and simultaneous REDOR distance measurements (*24*, *25*). Unexpected or unavoidable neighboring spin interactions may occur in unordered, nondilute samples or in labeled proteins, particularly if the folded structure is not known. Interference from ^{15}N–^{15}N interactions between enriched backbone amides is unlikely due to the low gyromagnetic ratio of ^{15}N and very weak homonuclear interaction strength. However, unexpected homonuclear ^{13}C interactions may be sufficiently strong to interfere with other measurements.

Our aim is to describe the effects of ^{13}C homonuclear interactions on ^{13}C{^{2}H} PM5-REDOR experiments for two different tripeptides, L-leucylalanylphenylalanine (LAF) and L-leucylglycylphenylalanine (LGF), labeled according to the scheme in Fig. 1. We demonstrate qualitative agreement between experimental data and simulated PM5-REDOR decay curves with ^{13}C homonuclear coupling interactions. The theoretical basis of the experimentally observed effects due to multiple spins is investigated. We also determine backbone torsion angles in the absence of additional spin-1/2 couplings, due to separation of the peptides in an environment of reorienting molecules.

RESULTS AND DISCUSSION

^{13}C{^{2}H} REDOR Decay Curves

The ^{13}C{^{2}H} PM5-REDOR decay curves of Fig. 2 show two experimental dephasing curves for each labeled tripeptide. The data represented by filled squares are dubbed LAF_{after} and LGF_{after}. Presence of a "before" suffix indicates the state of the samples shortly following purification by preparative HPLC and lyophilization. The "after" subscript refers to the samples after a period of time on the order of weeks after preparation. LAF_{before} and LGF_{before} have significantly different REDOR decay curves (Fig. 2, open circles) than the after peptides and theoretical decay curves (solid curves). This difference is most pronounced in the three-spin case of glycine (Fig. 2b). The LAF_{before} and LGF_{before} ^{13}C{^{2}H} PM5-REDOR decay curves do not decay to zero; they level off at approximately 0.2 on the normalized $S(t)/S_0(t)$ y-axis of Fig. 2.

The torsion angle ϕ is the only free parameter of the calculated ^{13}C{^{2}H} PM5-REDOR decay curves. Other parameters necessary for the calculations are identical to the previously published description (*13*). The experimental decay curves which best match the after samples are indicated by the theoretical curves shown in bold. The data for the peptide LGF_{after} is new and gives $\phi_{Gly} = \pm 70 \pm 10°$. Values for LAF_{after} were previously published (*13*); the bold curve in Fig. 2a is for the downfield peak at 170.7 ppm and corresponds to $\phi_{Ala} = +175 \pm 15°$.

^{15}N{^{2}H} REDOR Decay Curves

The ^{15}N{^{2}H} PM5-REDOR decay curves of LAF_{before} and LGF_{before} (open circles) and of LAF_{after} and LGF_{after} (filled squares) are given in Fig. 3. The data of Fig. 3a are smoothed with five-point adjacent averaging. The torsion angle ψ_i is the

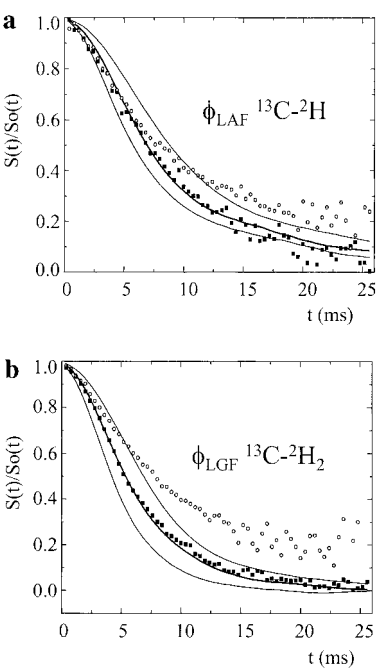

FIG. 2. ^{13}C-Observed, ^{2}H-dephased PM5-REDOR decay curves of (a) LAF and (b) LGF. Experimental dephasing of the before samples is shown as open circles. Filled squares represent the experimental decay of the after samples. Simulated decay curves (solid curves) mark the limits of possible $^{13}C_{i-1}$–$^{2}H_{i}^{\alpha}$ dipolar couplings: the two-spin ($^{2}H^{\alpha}$-alanine) case varies from 127 to 290 Hz; the three-spin ($^{2}H_{2}^{\alpha}$-glycine) case varies from 146 to 234 Hz. The leveling-off at ~0.2 (open circles) is clear despite the decreased signal to noise after 15 ms resulting in experimental scatter.

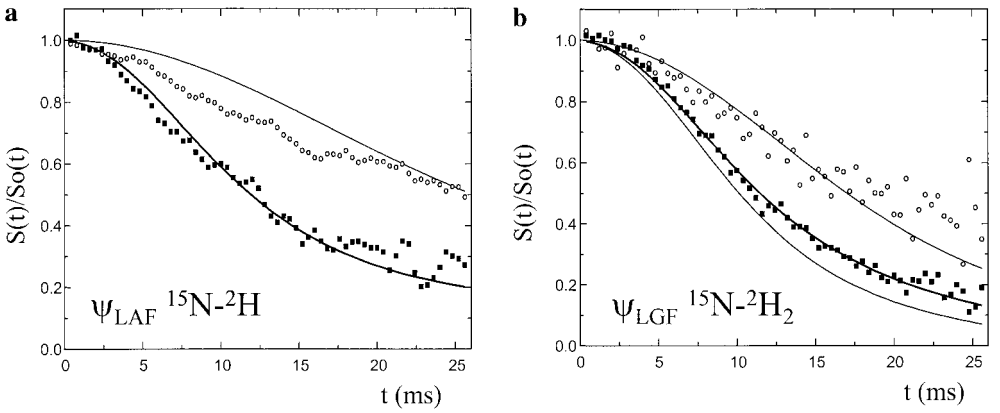

FIG. 3. ^{15}N-Observed, ^{2}H-dephased PM5-REDOR decay curves of (a) LAF and (b) LGF. Experimental dephasing of the before samples is shown as open circles. Filled squares represent the experimental decay of the after samples. Simulated decay curves (solid curves) mark the limits of possible $^{15}N_{i+1}$–$^{2}H_i^{\alpha}$ dipolar couplings: the two-spin ($^{2}H^{\alpha}$-alanine) case varies from 51 to 125 Hz; the three-spin ($^{2}H_2^{\alpha}$-glycine) case varies from 59 to 94 Hz. The experimental points in (a) are smoothed by five-point adjacent averaging.

only free parameter of the simulated ^{15}N{^{2}H} PM5-REDOR decay curve (solid curves) and is determined by comparisons with the experimental decay. The after samples can be described by the theoretical decay curves shown in bold. The LGF_{after} data are new and give $\psi_{Gly} = \pm 80 \pm 10°$. Values for LAF_{after} are reported elsewhere (*13*); the data shown in Fig. 3a give $\psi_{Ala} = +120 \pm 20°$.

The ^{15}N{^{2}H} PM5-REDOR dephasing of the before samples is within the range of the theoretical curves, yet does not follow any single curve. The decay curves of the before samples may be described by linear combinations of curves corresponding to multiple torsion angles arising from a sample of conformationally disperse peptides. It is not simple to deconvolute such curves. In particular the glycine residue can take on nearly any value. The torsion angles energetically allowed for L-amino acids are restricted by the amino acid side chains which sterically prohibit conformations in a manner described by Ramachandran plots (*26*, *27*). It was previously shown that correlating permitted ψ_i angles and corresponding PM5-REDOR decays place α-helices at the top of the graph with a slow decay curve and β-sheets at the opposite extreme with a relatively rapid decay curve (*13*). Many of the intermediate curves are sterically prohibited. A linear combination of multiple decay curves would thus contain torsion angles characteristic of both α-helix and β-sheet conformations, which is feasible for the before peptides based on the chemical shift values of the ^{13}C CPMAS spectra (*28*).

^{13}C/^{15}N CPMAS Spectra

The CPMAS spectra of before and after samples differ both in linewidths and in chemical shifts (Fig. 4). The linewidths of the before peptides are all much broader than the after peptides, suggesting that the before peptide samples are conformationally disperse. The CPMAS peaks correspond to a faster free-induction decay than the T_2 relaxation times measured with the $S_0(t)$ experiment (Table 1). The chemical shift differences suggest a conformational change.

The ^{13}C CPMAS spectrum of LAF_{after} is interesting for the appearance of two peaks with different chemical shifts corresponding to two different ϕ_{Ala} angles (*13*). The ^{15}N CPMAS spectra show two well-separated peaks, one from the ^{15}N-labeled backbone amide of Phe and the other from the ^{15}N-enriched terminal amino group of Leu (Fig. 1). If peptide hydrolysis was responsible for the changes between the before and after peptides, it would be apparent in the ^{15}N CPMAS spectra as a loss of signal intensity at the amide backbone peak. Some hydrolysis may have occurred in the LAF_{after} sample, but there is no evidence of peptide hydrolysis in the LGF_{after} sample.

Peptide Dynamics

To check for peptide dynamics, low-temperature ^{13}C{^{2}H} PM5-REDOR experiments at ~200 K were performed on LAF_{before}. The linewidths (and PM5-REDOR decay curves) were indistinguishable from those of the room temperature experiment (data not shown). The broad LAF_{before} sample appears to be rigid.

The static ^{2}H spectrum of the LGF_{before} sample contains only rigid molecules while the LGF_{after} spectrum indicates a mobile fraction (Fig. 5). Although there is a dynamic fraction in the after peptides, most of the sample is rigid. The breadth of the powder pattern is 120 kHz. The fine features could originate from a superposition of two species or a small anisotropy of the quadrupolar tensor.

^{1}H spectra also demonstrate differences between the before and after samples. Sharp ^{1}H spectral components are present in LAF_{after} and LGF_{after} but are absent in the before samples (Fig. 6). A 2D ^{13}C–^{1}H HETCOR experiment showed that only the broad linewidth (rigid) protons participate in CP excitation (data not shown). The sharp (mobile) ^{1}H peaks extend across a

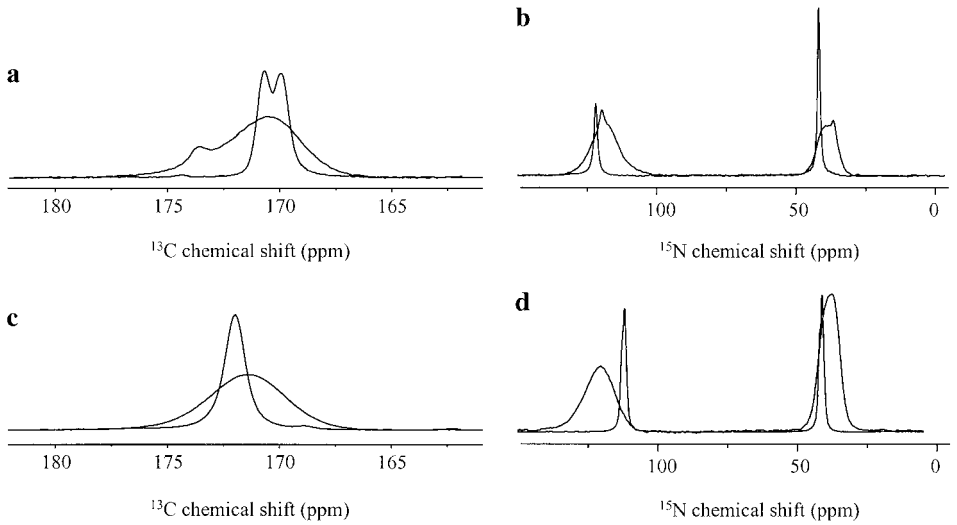

FIG. 4. A sum of 32 spectra obtained after ^{13}C or ^{15}N CPMAS–τ–echo–τ–AQ. Spectra were acquired with τ of 4–64 rotor periods, an 8-μs (^{13}C) π-pulse or a 16-μs (^{15}N) π-pulse, 65-kHz TPPM decoupling, and 5-kHz MAS. (a) ^{13}C LAF_{before} (broad) and LAF_{after} (narrow), (b) ^{15}N LAF_{before} (broad) and LAF_{after} (narrow), (c) ^{13}C LGF_{before} (broad) and LGF_{after} (narrow), (d) ^{15}N LGF_{before} (broad) and LGF_{after} (narrow). ^{15}N LAF_{after} is a single spectrum of 7000 scans using four rotor periods. The relative intensities of the backbone amide and the free amide peaks in LAF_{after} suggest that a fraction of the sample may be hydrolyzed. There is no evidence of hydrolysis in the LGF_{after} sample.

10-ppm range (Fig. 6, insets). A rapidly decaying peak ~4.8 ppm appearing in the ^{1}H spectra of the after peptides could be a water line. The presence of a water peak of similar magnitude to the other peaks would be consistent with the adsorption of molecular quantities of water.

To probe for mobility at the ^{13}C- or ^{15}N-labeled sites, direct 90° pulse excitation was compared to CP excitation experiments in the LGF_{after} peptide (Fig. 7). Both ^{13}C and ^{15}N 90° pulse excitation spectra reveal peaks not present in the CP excitation spectra. These spectra can be explained by the presence of a mobile peptide population in the after sample which does not participate in cross-polarization.

The relative intensities of the ^{13}C center bands are different between the two experiments (Fig. 7a). The data are consistent with mobile and rigid peptide populations that have the same ^{13}C isotropic chemical shift. Spinning sidebands are absent in the mobile fraction at the relatively low MAS frequency of 2 kHz due to motional averaging of the chemical shift anisotropy. The ^{13}C 90° pulse excitation spectrum was acquired with a repetition time between signal accumulations greater than T_1; thus the mobile fraction can be estimated by comparing integrated peak areas. This results in approximately 20% of the peptides in the LGF_{after} sample being mobile, consistent with the ^{1}H data.

The ^{15}N 90° pulse excitation spectrum of LGF_{after} shows two additional lines not present in the CPMAS spectrum (Fig. 7b). From the two different chemical shifts for each labeled ^{15}N we can deduce two peptide populations of different conformations. Interestingly, the chemical shifts of the mobile fraction appearing in the ^{15}N 90° pulse excitation spectrum match the CPMAS chemical shifts of LGF_{before} (Fig. 4d). The ^{15}N chemical shift data of Figs. 4 and 7 suggest that the LGF sample was initially

TABLE 1
Linewidths, T_2's, and Chemical Shifts of before and after Peptides

	^{13}C			^{15}N			
Tripeptide	$(\pi\Delta\nu)^{-1}$ (ms)	T_2 (ms)	Carbonyl σ (ppm)	$(\pi\Delta\nu)^{-1}$ (ms)	T_2 (ms)	Amide σ (ppm)	Amino σ (ppm)
LAF_{before}	1	10.8	170.5[a]	1	14.5	118.0	38.7
LGF_{before}	1	8.2	171.4	1	9.8	118.4	36.9
LAF_{after}	6	13.8	170.7[b]	7	22.6	119.1	42.3
LGF_{after}	5	10.6	172.0	10	40	111.0	41.1

Note. All linewidths are broader than the T_2's calculated from the S_0 (Hahn echo) experiments.
[a] There is also a shoulder at 173.6 ppm.
[b] This peak is plotted in Fig. 2. The upfield peak resonates at 170.0 ppm.

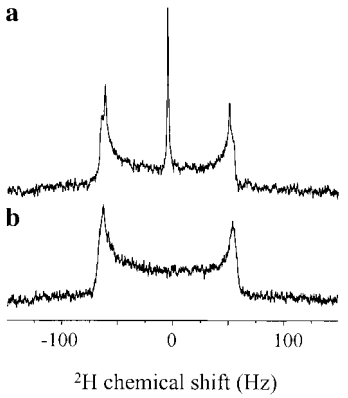

FIG. 5. Static ^{2}H spectra of (a) LGF_{after} and (b) LGF_{before}. A total of 28,000 transients were taken using a solid echo of two 90° pulses (2.5 μs each) and an echo delay of 100 μs.

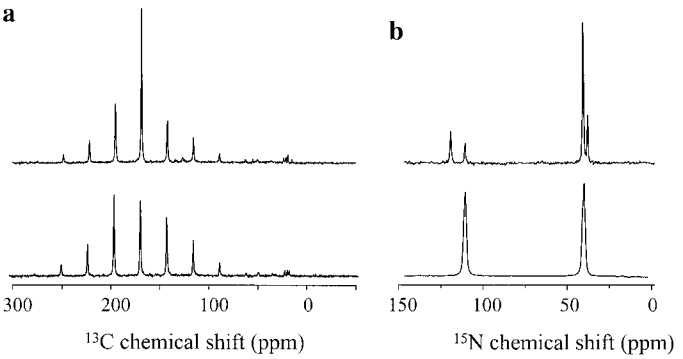

FIG. 7. 90° pulse excitation (top) vs CP excitation (bottom) of LGF_{after} peptides. (a) ^{13}C spectra acquired with 2-kHz MAS and (b) ^{15}N spectra acquired with 10-kHz MAS. The 30-s repetition delay of the 90° pulse excitation experiment was not sufficiently long to get the full intensity of the 111-ppm ^{15}N peak.

static with multiple small variations in conformation. With time, a minor fraction became mobile and most of the sample changed to a new static conformation. The long T_1 of the 111-ppm peak results in a reduced intensity in the direct excitation experiment and estimates of the mobile fraction cannot be made.

It is clear from the ^{2}H, ^{1}H, ^{13}C, and ^{15}N spectra that the after samples contain a mobile fraction. However, PM5-REDOR experiments are acquired with CP excitation and only the rigid population is observed.

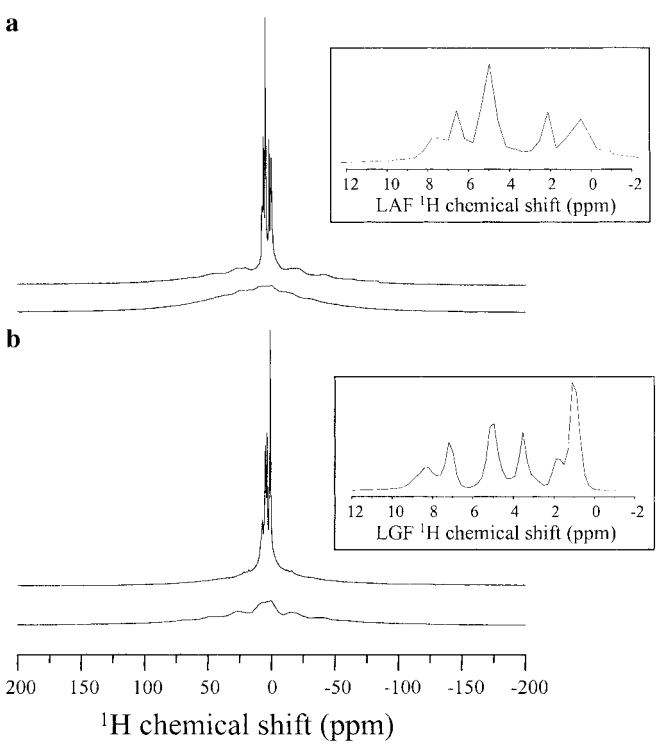

FIG. 6. ^{1}H 90° pulse excitation spectra of (a) LAF and (b) LGF at 5-kHz MAS. The broad lines correspond to the before samples. The after peptide spectra have narrow features which cover a chemical shift range approximately 0–10 ppm (enlarged in inset). The narrow peaks account for ~20% of the total integrated area of the after spectra.

^{13}C Homonuclear Interactions

Plotting the ^{13}C{^{2}H} PM5-REDOR decay curves of the individual $S_0(t)$ (reference) and $S(t)$ (PM5-REDOR) decays revealed unexpected results. The before and after peptides have very similar $S(t)$ decays while significant differences are apparent in the $S_0(t)$ decay (Figs. 8a and 8b). The reference experiment is simply CP excitation followed by a Hahn echo. Assuming the same T_2 for before and after ^{13}C peaks and taking the ratio $S_0(t)_{before}/S_0(t)_{after}$ results in an experimental ^{13}C decay curve which can be accounted for by homonuclear ^{13}C dipolar couplings and is independent of T_2 relaxation (Figs. 8a and 8b, open triangles).

Only *inter*molecular ^{13}C dipolar interactions are possible in the undiluted isotopically enriched peptides since each peptide contains only one ^{13}C specifically labeled carbon (Fig. 1). Reintroduction of homonuclear dipolar coupling during magic-angle spinning occurs at the rotational resonance condition $\Delta_{iso} = m\omega_R$, where the difference in isotropic chemical shifts between the two signals to be recoupled (Δ_{iso}) is equal to an integer multiple (m) of the spinning frequency (ω_R) (*29*). Dipolar interactions between ^{13}C pairs with the same isotropic chemical shifts but different orientations of the principal CSA tensors fulfill an $m = 0$ rotational resonance condition. Under $m = 0$ conditions homogeneously broadened linewidths gradually narrow with increasing MAS frequency until they are completely averaged with very fast spinning.

The spinning frequency dependent behavior at the rotational resonance condition of $m = 0$ of ^{13}C–^{13}C dipolar broadened linewidths was exploited to experimentally observe ^{13}C–^{13}C dipolar couplings in LAF_{before}. $S_0(t)$ (CPMAS–τ–180–τ–AQ) values were recorded at different spinning speeds (Fig. 9). Experimental decay values at 12 ms were divided by the

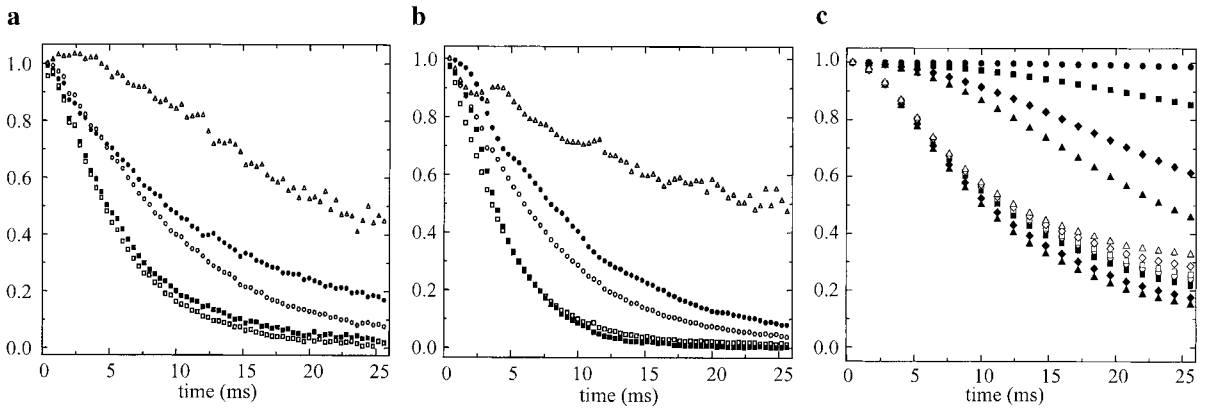

FIG. 8. Normalized decay curves of (a) LAF, (b) LGF, and (c) theory. The experimental data (a) and (b) are plotted with $S(t)_{\text{before}}$ = open squares, $S(t)_{\text{after}}$ = filled squares, $S_0(t)_{\text{before}}$ = open circles, and $S_0(t)_{\text{after}}$ = filled circles. The ratio $S_0(t)_{\text{before}}/S_0(t)_{\text{after}}$ (open triangles) is independent of T_2, assuming the same T_2 relaxation for both samples. The theoretical decay curves (c) are calculated using the LAF experimental parameters. Decay due to T_2 relaxation is not included in the simulations. Plotted are $S(t)$ (bottom set of filled symbols), $S_0(t)$ (top set of filled symbols), and $S(t)/S_0(t)$ (open symbols). The theoretical model allows one ^{13}C–^{2}H moiety to rotate around the σ_{yy} axis of its ^{13}C CSA tensor relative to an otherwise identical ^{13}C–^{2}H spin pair. Relative rotations are plotted for 20° = circles, 40° = squares, 60° = diamonds, and 80° = triangles. See the text for comparisons between experimental and theoretical curves.

10-kHz MAS value to remove T_2 effects. Simulations using SIMPSON (*30*) show that the data could be described by a single ^{13}C–^{13}C pair interaction with ~100-Hz dipolar coupling (Table 2). The simulations assumed the only interactions were between a central carbon and one, two, or three carbons equidistant to it. The carbons were all given the same chemical shift and CSA value. Simulations were run at a fixed distance, allowing only relative changes in CSA tensor orientations. Aligned tensors have no decay. Table 2 gives a distribution of values at the maximum extreme.

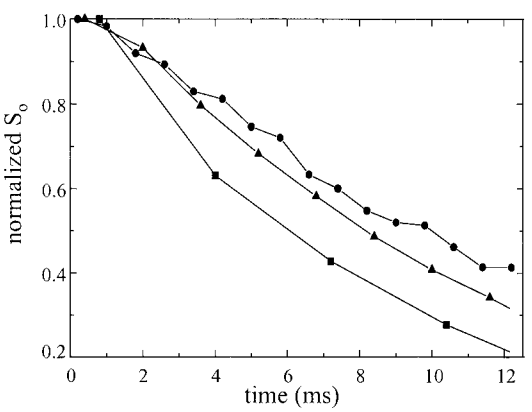

FIG. 9. Normalized ^{13}C $S_0(t)$ (CPMAS–τ–echo–τ–AQ) spectra from $\text{LAF}_{\text{before}}$ at three different spinning speeds: squares = 2.5-kHz MAS; triangles = 5-kHz MAS; circles = 10-kHz MAS; solid lines are only to guide the eye. The spinning speed dependent decay is due to an $m = 0$ rotational resonance between *inter*molecular ^{13}C carbonyl carbons. Table 2 compares the intensities, normalized to 10 kHz at 12 ms to remove T_2 contributions, between experiments and simulations. One or more ^{13}C pairs with ~100-Hz coupling can account for the observed homogeneous line broadening. An equivalent experiment observing ^{15}N did not display spinning speed dependent decay curves (data not shown).

Conformational Dispersion

The before powders were prepared by lyophilization of flash-frozen peptide solutions. It is conceivable that multiple solution-state conformations of the peptide are trapped in such a powder. It is known that lyophilized samples can have much broader solid-state NMR linewidths than precipitated solutions (*31, 32*) and that hydration can reduce conformational distributions (*33*). Each observed nucleus located in a slightly altered magnetic environment will resonate at a slightly different, unresolved chemical shift and produce broad lines.

It is expected that the putative trapped conformations of the peptides are not in their lowest energy states. LAF and LGF linewidth changes over time could result from the collapse of multiple unstable conformations to a single lower energy conformation. The conformationally equivalent molecules would share the same magnetic environment and resonate at a single chemical shift. Either this rearrangement itself or/and the environment of reorienting molecules observed in the after spectra as ~20% of the sample destroys close ^{13}C–^{13}C contacts. Narrow linewidths (~1 ppm) and the absence of ^{13}C homonuclear interactions result in ^{13}C{^{2}H} PM5-REDOR dipolar dephasing decays which can be analyzed simply. It may also be possible to combine PM5-REDOR with multiple-pulse decoupling (*34*) to extract quantitative results in the presence of additional spin-1/2 couplings.

Theoretical Background and Simulations

The REDOR evolution of a single $S = 1$ (^{2}H) to $I = \frac{1}{2}$ (^{13}C) coupled spin pair is complicated by the presence of homonuclear interactions between ^{13}C nuclei of neighboring ^{13}C–^{2}H pairs. To gain physical insight into the effect of these additional nuclear interactions on the experimental ^{13}C–^{2}H PM5-

TABLE 2
Normalized Experimental and Simulated ^{13}C Intensities at 12 ms

Coupling strength	Experimental[a]	Simulations[b]					
		119 Hz (4.0 Å)			90 Hz (4.4 Å)		
^{13}C interactions	N/A	1	2	3	1	2	3
I[c]	0.53	0.49	0.41	0.35	0.68	0.57	0.52
II[d]	0.78	0.82	0.74	0.67	0.90	0.83	0.77

[a] Experimental values are from Fig. 4.
[b] Euler angles are optimized to give maximum decay values using SIMPSON (*30*).
[c] Extent of peak intensity decay after 12 ms with 2.5-kHz MAS normalized to the decay at 10-kHz MAS to remove T_2 effects.
[d] Extent of peak intensity decay after 12 ms with 5-kHz MAS normalized to the decay at 10-kHz MAS to remove T_2 effects.

REDOR decay curves, we consider a small spin system of two interacting ^{13}C–^{2}H pairs. The influence of the ^{13}C–^{13}C dipolar coupling on the PM5-REDOR decay of this system will be discussed without attempting to derive analytical expressions for the decay functions.

The spin system under consideration consists of four spins: two ^{13}C spins ($I^1 = I^2 = \frac{1}{2}$) and two deuterons ($S^1 = S^2 = 1$). The system is restricted to magnetically equivalent carbons with identical isotropic chemical shifts and principal chemical shift tensor parameters. Consistent with the general case of $^{2}H^{\alpha}$-amino acids, each carbon atom is directly coupled to only one deuterium, I^1 to S^1 and I^2 to S^2. The internuclear distances within these pairs are equal. The deuterium quadrupolar interaction parameters are also equal. The magnitudes of the vectors connecting the carbon and deuterium atoms in each pair are equal, as well as their relative orientations with respect to their own quadrupolar principal axis system (PAS). The only permitted differences between the ^{13}C–^{2}H spin pair moieties will be their relative orientations around a fixed ^{13}C–^{13}C distance. For our discussion this simple model is sufficient to obtain insight into coherent evolution during $^{13}C\{^{2}H\}$ REDOR experiments.

The Hamiltonian of this system includes RF pulses only on the *S*-spins and can be written schematically as

$$H(t) = H^1_{\mathrm{RF}} + H^1_{\mathrm{Q}} + H^1_{IS} + H^1_{\mathrm{CSA}} + H^{12}_{II} + H^2_{\mathrm{CSA}} + H^2_{IS} + H^2_{\mathrm{Q}} + H^2_{\mathrm{RF}}, \quad [1]$$

where the first and the last terms, $H^{1,2}_{\mathrm{RF}}$, represent the RF pulses on S_1 and S_2, respectively; $H^{1,2}_{\mathrm{Q}}$ are the time-dependent quadrupolar MAS Hamiltonians; $H^{1,2}_{IS}$ are the time-dependent heteronuclear interactions between the carbon and deuteron for each of the two pairs

$$H^{1,2}_{IS} = \omega^{1,2}_{IS}(t) I^{1,2}_Z S^{1,2}_Z, \quad [2]$$

$H^{1,2}_{\mathrm{CSA}}$ indicate the time-dependent CSA MAS Hamiltonians of the carbons; and H^{12}_{II} is the time-dependent homonuclear MAS interaction Hamiltonian between the carbons

$$H^{1,2}_{II} = 2\omega^{12}_{II}(t) I^1_z I^2_z - \tfrac{1}{2}\omega^{12}_{II}(t)(I^1_+ I^2_- + I^1_+ I^2_-). \quad [3]$$

All of these terms are considered in our numerical calculations on the $(I^1S^1)(I^2S^2)$ spin system. For our discussion we can approximate the total Hamiltonian $H(t)$ by transforming it to a multispin interaction frame and considering only the zero-order part of the resulting Hamiltonian.

This was done in a recent publication for a single carbon–deuterium spin pair (*12*). There we transformed the dipolar part of the Hamiltonian to an interaction frame defined by the quadrupolar and RF Hamiltonians. Here we do the same for both spin pairs and define transformation operators starting with the *S*-spin subspace:

$$U_S(t) = T \exp\left\{ -i \int_0^t d\tau (H^1_{\mathrm{Q}}(\tau) + H^1_{\mathrm{RF}}(\tau) + H^2_{\mathrm{Q}}(\tau) + H^2_{\mathrm{RF}}(\tau)) \right\}. \quad [4]$$

An additional transformation operator can be defined in the *I*-spin subspace,

$$U_I(t) = \exp\left\{ -i \int_0^t d\tau (H^1_{\mathrm{CSA}}(\tau) + H^2_{\mathrm{CSA}}(\tau)) \right\}, \quad [5]$$

defined by the CSA Hamiltonians. While $U_S(t)$ commutes with $H^1_{\mathrm{CSA}} + H^{12}_{II} + H^2_{\mathrm{CSA}}$, the $U_I(t)$ operator commutes with all parts of the total Hamiltonian except H^{12}_{II}. The interaction Hamiltonian defined by both transformation operators,

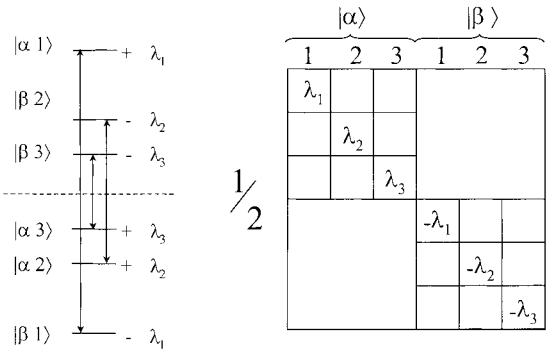

FIG. 10. An example of energy levels of an isolated I^1S^1 spin pair (left side), which illustrates the six eigenvalues of the diagonalized zero order Hamiltonian $\bar{H}_{IS}$ (right-hand side). The three frequency components comprising PM5-REDOR decays are indicated.

$$\tilde{H}(t) = U_I^{-1}(t)U_S^{-1}(t)(H_{IS}^1 + H_{IS}^2 + H_{II}^{12})U_S(t)U_I(t)$$
$$= \tilde{H}_{IS}(t) + \tilde{H}_{II}(t), \qquad [6]$$

has two terms, the heteronuclear and homonuclear interactions, respectively,

$$\tilde{H}_{IS}(t) = \omega_{IS}^1(t)I_z^1S_z^1(t) + \omega_{IS}^2(t)I_z^2S_z^2(t)$$
$$\tilde{H}_{II}(t) = 2\omega_{II}^{12}(t)I_z^1I_z^2$$
$$- \tfrac{1}{2}\omega_{II}^{12}(t)(I_+^1(t)I_-^2(t) + I_-^1(t)I_+^2(t)). \qquad [7]$$

The time dependence of the operators is a result of the $U_{I,S}(t)$ transformations. As long as the dipolar interaction coefficients are smaller than the spinning frequency and the detection is synchronous with the spinning, it should be sufficient to describe the REDOR experiments by a zero-order average Hamiltonian,

$$\bar{H} = \int_0^{T_R} d\tau\tilde{H}(\tau) = \bar{H}_{IS} + \bar{H}_{II}, \qquad [8]$$

where T_R is the time needed for one revolution of the rotor.

When the first term ($\bar{H}_{IS}$) is diagonalized in the manifold of spin states of each spin pair separately, the 12 eigenstates with eigenvalues (energies) are of the form $|\alpha^{1,2}p^{1,2}\rangle$ with $\frac{1}{2}\lambda_p^{1,2}$ and $|\beta^{1,2}p^{1,2}\rangle$ with $-\frac{1}{2}\lambda_p^{1,2}$ for the three S-state indices $p = 1, 2, 3$ (*12*). The magnitudes of these eigenvalues are determined by the quadrupolar and dipolar $I^{1,2}S^{1,2}$ tensor parameters in the rotating frame and depend on the shape and phases of the REDOR pulses on the S-deuterium spins.

Recently, we showed that PM5-REDOR pulses result in eigenvalues that increase the REDOR decay of powders containing ^{13}C–^{2}H spin pairs (*12*). A schematic representation of the eigenvalues of one of the spin pairs, together with the three transition frequencies that determine the REDOR oscillations of each crystallite in the powder, is presented in Fig. 10. To zero order, without a homonuclear interaction each *IS* spin pair contributes three cosine frequency terms of equal intensity to the REDOR signal of the I-spins. Thus, the two spin pairs contribute six frequencies for each crystallite. The two spin pairs have the same normalized REDOR powder decays, $S^{1,2}(nT_R)/S_0^{1,2}(nT_R)$. The powder signal of the two spin systems becomes

$$\frac{S^1(nT_R) + S^2(nT_R)}{S_0^1(nT_R) + S_0^2(nT_R)} = \frac{1}{24\pi^2}\int d\Omega \sum_{i=1}^{2}\sum_{p=1}^{3} \cos\lambda_p^i(\Omega)nT_R, \qquad [9]$$

where the orientational dependent eigenvalues $\frac{1}{2}\lambda_p^{1,2}(\Omega)$ are a function of the initial orientation Ω of the crystallites.

To show the validity of the zero-order approximation two simulated REDOR curves, one obtained from a zero order average Hamiltonian calculation in the interaction frame and one with a full stepwise integration in the rotating frame, are compared in Fig. 11. Although the two curves do not fully overlap, they are similar enough to justify a zero-order approach to understanding the spin evolution.

The presence of the *II* coupling requires that we combine the two eigenvalue schemes of the two *IS* spin pairs. The total number of states becomes 36,

$$|\alpha^1\alpha^2p^1q^2\rangle, |\alpha^1\beta^2p^1q^2\rangle, |\beta^1\alpha^2p^1q^2\rangle, |\beta^1\beta^2p^1q^2\rangle, \qquad [10]$$

where $p,q = 1, 2, 3$. Their undisturbed energy levels for each crystallite are $\pm\frac{1}{2}(\lambda_p^1(\Omega) \pm \lambda_q^2(\Omega))$.

The form of the zero-order time-independent *II* interaction Hamiltonian becomes

$$\bar{H}_{II} = \tfrac{1}{2}\bar{d}_{12}(\Omega)(I_+^1I_-^2 + I_-^1I_+^2). \qquad [11]$$

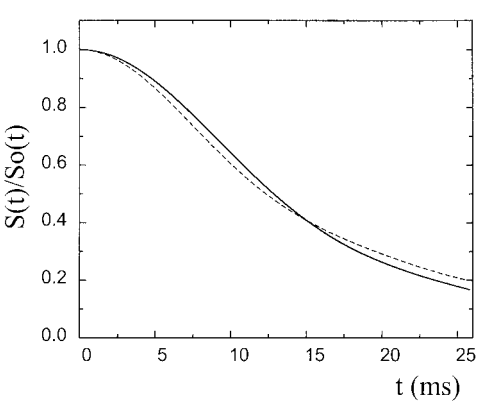

FIG. 11. Simulated PM5-REDOR decays of an *IS* spin pair. The solid curve was calculated using an approximate Hamiltonian while the dashed curve is a full calculation. The zero-order and full calculations are similar enough to justify a zero-order assumption.

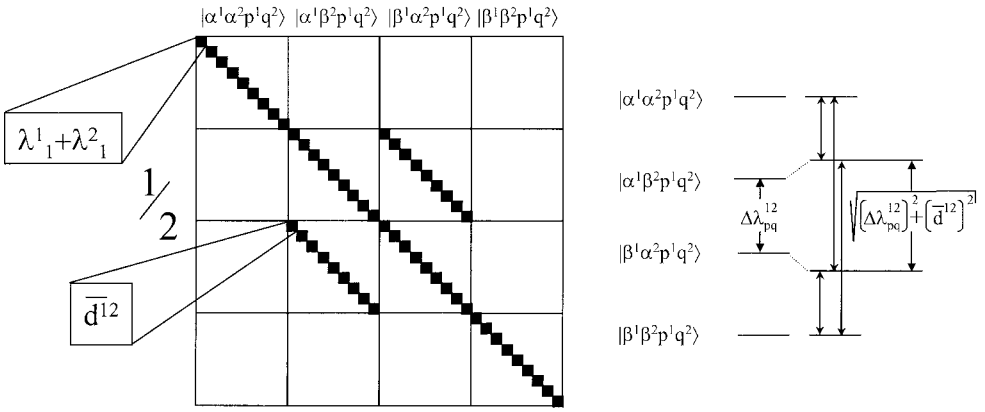

FIG. 12. Scheme of the zero-order Hamiltonians $\bar{H}_{I1S1} + \bar{H}_{I2S2} + \bar{H}_{II}$ of a four-spin system in the manifold of product spin states that diagonalize (left). The transition frequencies of one of nine sets of energy levels with and without influence of the homonuclear *II* interaction are shown on the right.

The value of its coefficient is proportional to the carbon–carbon dipolar interaction and is thus proportional to $(1/r_{12})^3$, with r_{12} the distance between the carbons. Furthermore, this coefficient is a complicated function of the CSA tensor parameter of the spins, and in our case of their relative orientation in each crystallite. In practice, only numerical calculations can yield the actual values of $\bar{d}_{12}(\Omega)$, taking into account all CSA parameters. When the principal values of the CSA tensors are equal, the coefficients depend strongly on the relative orientation of the two tensors and become zero when these tensors are aligned. In fact, an expression for $\bar{d}_{12}(\Omega)$ was derived earlier for the $m = 0$ rotational resonance condition (*35*).

The *II* interaction in Eq. [11] has matrix elements only between eigenstates in Eq. [10] that are diagonal in the *S*-spin states and connect $|\alpha^1\beta^2\rangle$ with $|\beta^1\alpha^2\rangle$. There are nine such pairs in the 36×36 matrix representation of the zero-order Hamiltonian (Fig. 12),

$$|\alpha^1\beta^2p^1q^2\rangle|\beta^1\alpha^2p^1q^2\rangle$$

$$\frac{1}{2}\begin{pmatrix} \lambda & \bar{d}_{12} \\ \bar{d}_{12} & -\lambda \end{pmatrix}, \qquad [12]$$

where the λ's are differences of the form $\lambda = (\lambda_p^1(\Omega) - \lambda_q^2(\Omega))$ and $\bar{d}_{12} = \bar{d}_{12}(\Omega)$. The off-diagonal elements will change the eigenvalues of the Hamiltonian and thus the overall REDOR signal. The six oscillation frequencies of the REDOR signal of each crystallite will therefore change according to the shifts of the eigenvalues to six different frequencies.

When the off-diagonal elements are much smaller than the differences between the eigenvalues of the individual carbon–deuterium spin pairs, their influence will be negligible. In general, the diagonal elements of these submatrices are nonzero. Only when the two *IS*-spin pairs are aligned can we expect that $\lambda_p^1(\Omega) = \lambda_p^2(\Omega)$. In this case the PAS of the CSA tensors are also aligned and the $\bar{d}_{12}(\Omega)$'s will become zero. In general, however, the complexity of the spin system will require numerical calculations to evaluate the λ-values and the effective carbon dipole–dipole couplings.

The effect of this *II* coupling on our REDOR decay curves is determined by the ratio between the $(\lambda_p^1(\Omega) - \lambda_q^2(\Omega))$ and the $\bar{d}_{12}(\Omega)$ values and can result in a quenching of the effective homonuclear interaction $\tilde{H}_{II}$ by the effective heteronuclear interaction $\tilde{H}_{IS}$. The ratio $(S^1(nT_R) + S^2(nT_R))/(S_0^1(nT_R) + S_0^2(nT_R))$ of the simulated curves (Fig. 8, open symbols) mimics the experimental leveling-off of $\text{LAF}_{\text{before}}$ (Fig. 2). Calculations for the four-spin system (^{2}H–^{13}C–^{13}C–^{2}H) used the full equation of motion of the density matrix.

Figure 8c plots theoretical curves as a function of the relative orientation of the CSA tensors between interacting carbons of neighboring ^{13}C–^{2}H spin systems. The calculations of $(S^1(nT_R) + S^2(nT_R))$, $(S_0^1(nT_R) + S_0^2(nT_R))$, and $(S^1(nT_R) + S^2(nT_R))/(S_0^1(nT_R) + S_0^2(nT_R))$ were made with a fixed ^{13}C–^{13}C distance (4.2 Å = 100 Hz). One ^{13}C–^{2}H moiety of the ^{13}C–^{13}C pair was rotated relative to the other around the σ_{yy} axis of its ^{13}C CSA tensor in steps of 20° (20–80°). The parameters used in the simulations are taken from the $\text{LAF}_{\text{before}}$ experiment shown in Fig. 8a. What results is relatively little change in the $(S^1(nT_R) + S^2(nT_R))$ decay curves (bottom set of solid symbols), whereas the Hahn echo decay signal of the interacting carbons $(S_0^1(nT_R) + S_0^2(nT_R))$ without REDOR pulses on the deuterons is strongly influenced by the homonuclear interaction (top set of solid symbols).

The calculated curves do not include T_2 relaxation. Taking ratios of experimental curves with the same T_2 relaxation removes T_2 effects. The experimental $S_0(t)_{\text{before}}/S_0(t)_{\text{after}}$ curves are remarkably similar to the theoretical $(S_0^1(nT_R) + S_0^2(nT_R))$ decay with an 80° difference between ^{13}C CSA tensor orientations. Similarities to the experimental curves are limited to qualitative interpretations, however, because of the complexity of the system.

CONCLUSIONS

The presence of *inter*molecular ^{13}C–^{13}C interactions prevents the $^{13}C\{^2H\}$ PM5-REDOR curves from decaying to zero. It is seen experimentally and theoretically that homonuclear ^{13}C spin interactions only significantly perturb the $S_0(t)$ (reference) experiments while effects on the $S(t)$ (PM5-REDOR) decays are small. A theoretical description of quenching of relatively weak ^{13}C–^{13}C interactions by the reintroduction of ^{13}C–^{2}H heteronuclear dipolar couplings in the $S(t)$ experiment was developed.

The broad lines of the lyophilized powders (^{13}C, ~4 ppm; ^{15}N, ~10 ppm) appear to originate from conformational dispersion. A slow conformational change of the entire sample (on the order of weeks) can explain the narrowed linewidths (^{13}C, ^{15}N, ~1 ppm). Disruption of molecular packing by conformational rearrangements in an environment of reorienting molecules in the after peptides appears to remove *inter*molecular ^{13}C–^{13}C interactions, allowing $^{13}C\{^2H\}$ PM5-REDOR dipolar dephasing curves to decay to zero. The peptide torsion angles ϕ and ψ of the after tripeptides were determined using PM5-REDOR.

The mobile fraction of LAF_{after} and LGF_{after} peptides (~20%) does not participate in CP. The $^{13}C\{^2H\}$ PM5-REDOR experiments are unaffected by this mobile population since CP excitation serves as a mobility filter. This project demonstrated the advantages of multiple labels within a single peptide sample for providing complementary spectroscopic probes into peptide structure and dynamics.

EXPERIMENTAL

The standard FMOC synthesis and HPLC purification of L-[1-^{13}C, ^{15}N]Leu-[2-^{2}H]Ala-[^{15}N]Phe (LAF) was previously described in detail (*13*), L-[1-^{13}C, ^{15}N]Leu-[2-$^{2}H_2$]Gly-[^{15}N]Phe (LGF) was synthesized and purified in an identical manner in parallel. Purified peptides (>89%) were lyophilized overnight and packed into Bruker zirconia rotors fitted with Kel-F end caps.

After tripeptide synthesis, purification, and lyophilization, identical fractions of the LAF_{before} sample were packed into a 4- and 7-mm rotors. After about 1 month, changes in the PM5-REDOR decay, spectral linewidths and positions of the 7-mm rotor LAF sample prompted questions into the differences between LAF_{before} and LAF_{after}. Relyophilization of a moistened LAF sample in the 4-mm rotor appeared to prolong the characteristics described as LAF_{before}, although slow changes in this sample were eventually observed as well. The LGF_{before} sample was initially packed into a 7-mm rotor. After 4 months the sample was transferred to a 4-mm rotor. The observed spectral changes in LGF mirrored what had occurred in the LAF sample. Our final samples were therefore LAF_{before} (4-mm rotor), LAF_{after} (7-mm rotor), LGF_{before} (7-mm rotor), and LGF_{after} (4-mm rotor).

A Bruker DSX-300 spectrometer was used for all experiments. ^{1}H (300.13 MHz) spectra were calibrated to an external adamantine sample at 1.8 ppm. ^{13}C (75.47 MHz) spectra were calibrated to an external glycine carbonyl chemical shift of 176.04 ppm. ^{15}N (30.41 MHz) spectra were calibrated to an external solid NH_4Cl sample at 38.5 ppm. ^{2}H (46.07 MHz) dephasing used phase-modulated (PM5) pulses. Acquisition parameters for the PM5-REDOR measurements under 5-kHz MAS and numerical simulations of the data were identical to the previously published description (*13*).

ACKNOWLEDGMENTS

This work was supported by a grant from the German–Israeli Science Foundation. I.S. was supported by the MINERVA foundation. We thank Gerd Buntkowsky and Asher Schmidt for helpful discussions.

REFERENCES

1. J. R. Garbow and T. Gullion, Measurement of internuclear distances in biological solids by magic-angle spinning 13C NMR, *in* "Carbon-13 NMR Spectroscopy of Biological Systems" (N. Beckman, Ed.), pp. 65–115, Academic Press, San Diego, 1995.
2. R. G. Griffin, Dipolar recoupling in MAS spectra of biological solids, *Nat. Struct. Biol.* **5,** 508–512 (1998).
3. R. Q. Fu and T. A. Cross, Solid-state nuclear magnetic resonance investigation of protein and polypeptide structure, *Annu. Rev. Biophys. Biomol. Struct.* **28,** 235–268 (1999).
4. B. Bechinger, R. Kinder, H. Helmle, T. C. B. Vogt, U. Harzer, and S. Schinzel, Peptide structural analysis by solid-state NMR spectroscopy, *Biopolymers* **51,** 174–190 (1999).
5. T. Gullion and J. Schaefer, Rotational-echo-double resonance NMR, *J. Magn. Reson.* **81,** 196–200 (1989).
6. A. Schmidt, T. Kowalewski, and J. Schaefer, Local packing in glassy polycarbonate by carbon deuterium REDOR NMR, *Macromolecules* **26,** 1729–1733 (1993).
7. T. Gullion, Measurement of dipolar interactions between spin-1/2 and quadrupolar nuclei by rotational-echo, adiabatic-passage, double-resonance NMR, *Chem. Phys. Lett.* **246,** 325–330 (1995).
8. D. Sandstrom, M. Hong, and K. Schmidt-Rohr, Identification and mobility of deuterated residues in peptides and proteins by H-2–C-13 solid-state NMR, *Chem. Phys. Lett.* **300,** 213–220 (1999).
9. T. Gullion, A comparison between REDOR and theta-REDOR for measuring C-13–D-2 dipolar interactions in solids, *J. Magn. Reson.* **139,** 402–407 (1999).
10. I. Sack, A. Goldbourt, S. Vega, and G. Buntkowsky, Deuterium REDOR: Principles and applications for distance measurements, *J. Magn. Reson.* **138,** 54–65 (1999).
11. B. Kesling, E. Hughes, and T. Gullion, ^{13}C–^{14}N REAPDOR and ^{13}C–^{2}D θ-REDOR NMR on a blend of tri-*p*-tolylamine and bisphenol-*A*-polycarbonate, *Solid State Nucl. Magn. Reson.* **16,** 1–7 (2000).
12. I. Sack and S. Vega, Efficient deuterium–carbon REDOR NMR spectroscopy, *J. Magn. Reson.* **145,** 52–61 (2000).
13. I. Sack, Y. S. Balazs, R. Rahimipour, and S. Vega, Solid-state NMR determination of peptide torsion angles: Applications of 2H-dephased REDOR, *J. Am. Chem. Soc.,* in press (2000).
14. R. Tycko, D. P. Weliky, and A. E. Berger, Investigation of molecular structure in solids by two-dimensional NMR exchange spectros-

copy with magic angle spinning, *J. Chem. Phys.* **105,** 7915–7930 (1996).

15. M. Hong, J. D. Gross, and R. G. Griffin, Site-resolved determination of peptide torsion angle phi from the relative orientations of backbone N–H and C–H bonds by solid-state NMR, *J. Phys. Chem. B* **101,** 5869–5874 (1997).
16. M. Hong, J. D. Gross, C. M. Rienstra, R. G. Griffin, K. K. Kumashiro, and K. Schmidt-Rohr, Coupling amplification in 2D MAS NMR and its application to torsion angle determination in peptides. *J. Magn. Reson.* **129,** 85–92 (1997).
17. J. Heller, D. D. Laws, M. Tomaselli, D. S. King, D. E. Wemmer, A. Pines, R. H. Havlin, and E. Oldfield, Determination of dihedral angles in peptides through experimental and theoretical studies of alpha-carbon chemical shielding tensors, *J. Am. Chem. Soc.* **119,** 7827–7831 (1997).
18. P. R. Costa, J. D. Gross, M. Hong, and R. G. Griffin, Solid-state NMR measurement of Psi in peptides: A NCCN 2Q-heteronuclear local field experiment, *Chem. Phys. Lett.* **280,** 95–103 (1997).
19. P. R. Costa, D. A. Kocisko, B. Q. Sun, P. T. Lansbury, and R. G. Griffin, Determination of peptide amide configuration in a model amyloid fibril by solid-state NMR, *J. Am. Chem. Soc.* **119,** 10487–10493 (1997).
20. X. Feng, M. Eden, A. Brinkmann, H. Luthman, L. Eriksson, A. Graslund, O. N. Antzutkin, and M. H. Levitt, Direct determination of a peptide torsional angle psi by double-quantum solid-state NMR, *J. Am. Chem. Soc.* **119,** 12006–12007 (1997).
21. P. V. Bower, N. Oyler, M. A. Mehta, J. R. Long, P. S. Stayton, and G. P. Drobny, Determination of torsion angles in proteins and peptides using solid state NMR, *J. Am. Chem. Soc.* **121,** 8373–8375 (1999).
22. K. Nomura, K. Takegoshi, T. Terao, K. Uchida, and M. Kainosho, Determination of the complete structure of a uniformly labeled molecule by rotational resonance solid-state NMR in the tilted rotating frame, *J. Am. Chem. Soc.* **121,** 4064–4065 (1999).
23. D. C. Muchmore, L. P. McIntosh, C. B. Russell, D. E. Anderson, and F. W. Dahlquist, Expression and N-15 labeling of proteins for proton and N-15 nuclear magnetic resonance, *Methods Enzymol.* **177,** 44–73 (1989).
24. T. Gullion and C. H. Pennington, θ-REDOR: An MAS NMR method to simplify multiple coupled heteronuclear spin systems, *Chem. Phys. Lett.* **290,** 88–93 (1998).
25. O. Liivak and D. B. Zax, Multiple simultaneous distance determinations: Application of rotational echo double resonance nuclear magnetic resonance to IS_2 spin networks, *J. Chem. Phys.* **113,** 1088–1096 (2000).
26. G. N. Ramachandran, C. Ramakrishnan, and V. Sasisekharan, Stereochemistry of polypeptide chain configurations, *J. Mol. Biol.* **7,** 95–99 (1963).
27. G. N. Ramachandran and V. Sasisekharan, Conformation of polypeptides and proteins, *Adv. Protein Chem.* **23,** 283–437 (1968).
28. H. Saito, Conformation-dependent ^{13}C chemical shifts: A new means of conformational characterization as obtained by high-resolution solid-state NMR, *Magn. Reson. Chem.* **24,** 835–852 (1986).
29. D. P. Raleigh, M. H. Levitt, and R. G. Griffin, Rotational resonance in solid state NMR, *Chem. Phys. Lett.* **146,** 71–76 (1988).
30. M. Bak, J. T. Rasmussen, and N. C. Nielsen, SIMPSON: A general program for solid-state NMR spectroscopy, *J. Magn. Reson.* **147,** 296–330 (2000) http://nmr.imsb.au.dk.
31. J. Pauli, B. van Rossum, H. Forster, H. J. M. de Groot, and H. Oschkinat, Sample optimization and identification of signal patterns of amino acid side chains in 2D RFDR spectra of the α-spectrin SH3 domain, *J. Magn. Reson.* **143,** 411–416 (2000).
32. Y. Tomita, E. J. O'Connor, and A. McDermott, A method for dihedral angle measurement in solids—Rotational resonance NMR of a transition state inhibitor of triose phosphate isomerase, *J. Am. Chem. Soc.* **116,** 8766–8771 (1994).
33. R. B. Gregory, M. Gangoda, R. K. Gilpin, and W. Su, The influence of hydration on the conformation of lysozyme studied by solid-state ^{13}C-NMR spectroscopy, *Biopolymers* **33,** 513–519 (1993).
34. J. Schaefer, REDOR-determined distances from heterospins to clusters of C-13 labels, *J. Magn. Reson.* **137,** 272–275 (1999).
35. G. Goobes, G. J. Boender, and S. Vega, Spinning frequency dependent narrowband RF-driven dipolar recoupling, *J. Magn. Reson.* **146,** 204–219 (2000).